


Reflectance confocal microscopy for noninvasive examination of nonmelanocytic tumors and virus-associated skin lesions in organ transplant recipients

Lena Rueter¹ | Pierluigi Ramadori² | Martina Ulrich³ | Sora Jung¹  | Bernd Kardorff⁴ | Juergen Lademann¹

¹Department of Dermatology, Venerology and Allergology, Berlin Institute of Health, Corporate Member of Freie Universität Berlin, Humboldt-Universität zu Berlin, Charité Universitätsmedizin Berlin, Berlin, Germany

²Division of Chronic Inflammation and Cancer, German Cancer Research Center, Heidelberg, Germany

³CMB Collegium Medicum Berlin, Berlin, Germany

⁴Gemeinschaftspraxis für Dermatologie, Allergologie, Phlebologie und Umweltmedizin Mönchengladbach, Mönchengladbach, Germany

Correspondence

Sora Jung, Department of Dermatology, Venerology and Allergology, Berlin Institute of Health, Corporate Member of Freie Universität Berlin, Humboldt-Universität zu Berlin, Charité – Universitätsmedizin Berlin, Berlin, Germany.
Email: sora.jung@charite.de

Abstract

Background: Drug-induced immunosuppression is necessary to prevent rejection of the foreign organ in transplanted patients, but neoplastic and virus-associated skin diseases are frequent complications. Reflectance confocal microscopy (RCM) recently emerged as a promising tool for the early diagnosis of skin lesions.

Materials and methods: A total of 61 skin lesions, among them 20 basal cell carcinomas, six Bowen's diseases, 23 actinic keratoses, and 12 verrucae, were analyzed. All lesions were clinically evaluated followed by RCM evaluation by two independent dermatologists and histological examination.

Results: For the diagnosis of basal cell carcinoma, a sensitivity of 100% by both investigators (INV I + II) and a specificity of 100% by INV I and 80% by INV II were achieved. The sensitivity average rate for RCM features reached by both investigators ranged between 60% and 100%, and the specificity between 55% and 90%. For the diagnosis of actinic keratosis, a concordant sensitivity of 94.4% and a specificity of 80% (INV I) and 60% (INV II) were detected. The sensitivity average rate of specific RCM criteria ranged between 72.3% and 97.2%, whereas specificity ranged between 20% and 90%. Regarding verrucae, RCM confirmed the histological diagnosis with a sensitivity of 85.7% (INV I) and 100% (INV II), while specificity was 100% and 80%, respectively.

Conclusion: Reflectance confocal microscopy resulted to be a reliable tool for the noninvasive diagnosis of neoplastic and virus-associated skin changes in organ transplant recipients. Nevertheless, given the frequency and diagnostic complexity of the hyperkeratotic lesions occurring post-transplantation, larger cohorts of patients are required to confirm and consolidate these findings.

KEYWORDS

basal cell carcinoma, Bowen's disease, epithelial skin cancer, immunosuppression, reflectance confocal microscopy, verrucae

This is an open access article under the terms of the Creative Commons Attribution License, which permits use, distribution and reproduction in any medium, provided the original work is properly cited.

© 2019 The Authors. *Skin Research and Technology* published by John Wiley & Sons Ltd

1 | INTRODUCTION

An organ transplantation is considered to be a life-saving procedure for patients with severest organ damage. The continuous intake of various immunosuppressants can prevent a rejection of the foreign organ by the patient's own immune system. The number of organ transplanted patients has increased to 1 000 000 worldwide.¹ Verrucae and skin tumors are the two most frequent skin diseases in organ transplanted patients, with skin tumors also accounting for 40%-50% of the malignant tumors. The malignant tumor incidence increases with the duration of the immunosuppressive therapy. In Western Europe and in the United States, 5% of all organ transplant recipients are suffering from malignant skin tumors in the first year post-transplantation. 10 years after the transplantation 10%-27% and after 20 years 40%-60% of the patients are affected. In Australia, the tumor incidence after 20 years even increases to 70%-82%,² with the risk of nonmelanocytic skin tumors being especially high. These tumors account for 95% of all skin tumors in long-term transplant recipients.³ In addition, multiple lesions in the sense of a field cancerization are often detectable in nonmelanocytic skin tumors in organ transplant recipients. The mortality rate of immunosuppressed patients is also increased, exceeding 5%.⁴ Verrucae and skin tumors in organ transplanted patients occur at different times in the corresponding skin areas, with over 90% of the skin tumors manifesting in UV-exposed skin areas.^{5,6} Moreover, the type, dose, and length of immunosuppressive treatment, an increased age of the patient at transplantation, the kind of the transplanted organ, and dialysis prior to kidney transplantation play an important role.^{4,7,8} The prognosis for neoplastic and virus-associated skin diseases in immunocompetent patients can be excellent, provided these diseases are diagnosed and treated in an early stage. In organ transplant recipients, however, it is to be considered that even inconspicuous skin lesions tend to quickly progress and infiltrate deeply. These skin diseases often occur in multiple number at unusual locations, and in many cases, their morphology is atypical. Therefore, they may present a considerable diagnostic challenge for the investigator. Diagnostic problems may occur especially when it comes to micronodular basal cell carcinoma (BCC) in the face which is frequently associated with multiple benign hyperplasia of the sebaceous glands that are also generated under immunosuppression, to sclerodermiform BCCs or to superficial BCCs without any dermatoscopic criteria.⁹ The current diagnostic standard consists of a histological examination after invasive skin biopsy. In general, an in situ squamous cell carcinoma (SCC), which is divided into actinic keratosis (AK) and its specific form of Bowen's disease, is clinically diagnosed. However, since it is often impossible to distinguish between an in situ and an early invasive SCCs, the histological evaluation remains to be the gold standard.^{10,11} Furthermore, verrucae are also clinically diagnosed. However, if the mostly hyperkeratotic lesions cannot be distinguished from AKs and early invasive SCCs by differential diagnostics, a sample should be excised in these specific cases, too.¹² Compared with the non-transplanted test population, the incidence of BCC in organ transplanted patients is 10 times higher.¹³

In addition, their risk of developing AK is 250-fold higher and their risk of an invasive SCC genesis is 100 times higher.¹⁴ Within the first 5 years of immunosuppression, 40% of all organ transplanted patients are developing AKs.⁴ Overall, it can be said that it is necessary to repeatedly excise multiple skin samples from organ transplanted patients. For this patient cohort, it also has to be considered that they often receive a continuous co-medication with an anticoagulant, which may result in an increased risk of bleeding. Due to the chronic immunosuppression, the risk of wound infections in the surgery area is increased. Thus, the development of reliable noninvasive and time-saving investigation methods is indispensable as an alternative to routine histology. Reflectance confocal laser scanning microscopy (RCM) is an optical high-resolution noninvasive diagnostic procedure permitting the visualization of dermatological processes at a cellular level. Like an in vivo biopsy, it enables in real time to image epidermal and superficial dermal structures down to the upper stratum reticulare.^{15,16} Since organ transplanted patients are often showing widespread extensions of the skin changes and subclinical lesions, RCM can be used to determine the most suitable biopsy site. In this way, scars caused by unnecessary invasive biopsies are avoided. In recent years, the applicability of RCM for in vivo diagnostics of neoplastic and virus-associated skin changes in immunocompetent patients was investigated. In all studies, this method was described as a promising tool for noninvasive diagnostics.¹⁷⁻²⁴ The confocal microscopic evaluation criteria of BCC are well known.^{18,25-29} Most of them become visible at the level of the superficial dermis (D) and the dermo-epidermal junction (DEJ), respectively.³⁰ A large multicenter study showed high sensitivity and specificity values for selected parameters, which correlated well with those of the conventional histology.¹⁸ On the other hand, there are only a few studies, so far, that used RCM to evaluate Bowen's disease.^{19,31-34} Investigations of Ulrich et al demonstrated that the RCM parameters of Bowen's disease resembled those of AK.^{19,31} Characteristic RCM criteria for AK can be derived from many publications.^{17,20,35-37} Horn et al and Ulrich et al could obtain for these criteria high sensitivity and specificity values in two independent studies. Moreover, the parameters were shown to correlate well with the established histological criteria.^{17,20} Only a few authors used RCM for evaluating verrucae. Examinations of verrucae plantares, verrucae planae, and condylomata acuminata have been published,²¹⁻²⁴ but the number of studies on RCM criteria of verrucae is rather limited.

The purpose of the present study was to assess the accuracy of RCM for the diagnosis of neoplastic and virus-associated skin changes in organ transplanted patients by using selected RCM evaluation criteria in a clinical setting. The gold standard was the conventional routine histology. In the initial experiments, the hitherto published RCM criteria of the individual skin changes were reproduced. Subsequently, the sensitivity and specificity data were determined for both the RCM diagnosis and the individual parameters. Finally, it was assessed whether the investigators had reached concordant results. The method is supposed to be highly reliable if all RCM criteria are detected by the independent investigators (INVs) and concordant RCM diagnoses are made, respectively.

2 | MATERIALS AND METHODS

2.1 | Patients

Once the approval of the competent ethics committee had been obtained, the study participants were recruited at the Skin Tumor Center of the Charité—Universitätsmedizin Berlin. The patients were examined during their risk profile-adapted prophylactic checkups and follow-ups, respectively. A total number of 35 patients, nine of them female and 26 of them male patients, with skin types I-III according to the Fitzpatrick scale, aged between 46 and 83 years (mean of 64.5 years) were included in the study. Thirty one of these patients had a kidney transplant, three a heart transplant, and one patient had simultaneously received a kidney and a heart transplant. Overall, 61 skin changes were clinically, dermatoscopically, confocal microscopically, and histologically evaluated. 20 lesions were considered suspicious for BCC, six for Bowen's disease. AK was clinically diagnosed 23 times, and 12 skin lesions appeared as verrucae.

2.2 | Evaluation by reflectance confocal microscopy

At first, a dermatoscopic image (VivaCam®) of the skin change was made, which was then evaluated using RCM (VivaScope®). Thereby, the dermatoscopic images and RCM images were superimposed so that a concordance between the images was obtained. With the VivaBlock® function, horizontal maps were captured at the levels of the stratum spinosum (SS) and the superficial dermis. In addition, one VivaStack®, each, was generated at 5- μm intervals down to the maximum depth of 250 μm , that is, from the stratum corneum (SC) through the entire epidermis, down to the level of the upper papillary dermis, with extra single images being taken in the areas of specific interest. The video capture module was used to produce short videos at the DEJ/D level, where vessels were observed, in order to visualize the blood flow.

2.3 | Histology

To confirm the suspected clinical diagnosis and the correlation of the RCM findings with the criteria of the conventional histology, a sample was biopsied. The punch biopsy diameter was 4-6 mm, on average. Subsequently, the specimen was evaluated at the division of dermatohistology of the Charité—Universitätsmedizin Berlin. In the clinically suspected BCC cohort, the diagnosis could be confirmed by the histological result 10 times, whereas 10 further lesions were found to be other benign and malignant skin changes (non-BCC lesions). In the Bowen cohort, the clinical diagnosis for 4 out of 6 lesions was confirmed by histology. In the cohort with clinically suspected AKs, the diagnosis could be histologically confirmed for 18 out of 23 lesions. The verruca cohort included 12 lesions, seven of which were verrucae and five non-verrucae.

2.4 | Morphological analyses

The RCM images were retrospectively subjected to a morphological analysis by two independent dermatologists (INV I and INV II). One investigator was already well versed in RCM, whereas the skills of the second investigators were considered to be moderate. Thereby, it was possible to create study conditions reflecting the overall dermatological community that consists of investigators with different RCM experience. The INVs were aware of the suspected clinical diagnosis. The lesions were morphologically described and systematically evaluated for the presence and absence, respectively, of specific RCM criteria for each diagnosis, which are known in the current literature. If $\geq 50\%$ of the generally described RCM criteria were found, the clinical diagnosis was confirmed by RCM.

2.5 | Technical principles of reflectance confocal microscopy

The reflectance confocal microscope (RCM) consists of a light source, a focusing and an objective lens, and a detector.¹⁶ A diode laser beam serves as source for monochromatic, coherent light which penetrates into the skin through a beam splitter and the objective lens and focuses a small spot in the tissue.¹⁵ Contrary to histology with its established vertical incision, the laser of the RCM scans in horizontal direction. Thus, the image interpretation is based on virtual horizontal tissue incisions.³⁸ The light is reflected, scattered, or absorbed by various refractive indices on boundary layers, cell organelles, and cellular microstructures.³⁹ The light signals reflected from the skin return to the detector in front of which a tiny pinhole aperture is installed. This ensures that only light from the focused level is processed.¹⁵ Subsequently, the light signals are transferred to a computer that generates two-dimensional sectional images of various gray shades from the differentiated reflexion patterns.⁴⁰ Thereby, the contrast of the RCM images is based on the different refractive indices of "endogenous contrast media".³⁹ Structures with a high refractive index result in a bright confocal image.¹⁵ With a refractive index of $n = 1.72$, melanin is the strongest contrast provider. Further natural contrast media are keratin ($n = 1.51$) and hydrogenated collagen ($n = 1.43$). They are surrounded by structures with a lower refractive index, such as epidermis ($n = 1.34$) and dermis ($n = 1.41$).^{16,38} In this study, a commercial RCM suitable for in vivo application (VivaScope® 1500; Lucid-Tech Inc, MAVIG GmbH) was used. The laser energy at tissue level is below 30 mW, thus not inducing any tissue or eye damage (laser category Ia).³⁸ The lateral resolution is $< 1.25 \mu\text{m}$, thus being at cellular level. The lateral resolution is around $< 5 \mu\text{m}$, thus corresponding approximately to the layer thickness of conventional histology.^{15,41} Skin structures can be represented down to a total penetration depth of 250-350 μm .³⁹ By positioning the VivaCam® onto a stainless steel ring, which is fixed to the patient's skin area, a digital image of dermatoscopic quality can be

generated. The macrocamera generates single images of 5 megapixel size on a 10 x 10 mm image area and ensures a correlation of the macroscopic images with the confocal images of the VivaScope®. By displacing the x-, y-, and z-axes of the laser, imaging at three levels is possible. Single images are 500 x 500 µm in size. By moving the x- and y-axes of the laser, a skin layer of maximally 8 x 8 mm in size can be scanned. In this way, a map of 16 x 16 single images is generated which corresponds to a VivaBlock®. The resolution of VivaBlocks® is 2 pixel/µm. The VivaStack® function generates images in the z-axis, thus providing an optical punch biopsy. VivaCube® combines VivaBlock® with VivaStack®. This function permits to completely scan a skin area in the x, y, and z directions (length x width x depth).^{38,42}

2.6 | Statistical analysis

Statistical data evaluation was conducted using the statistic programs GraphPad Prism 7 and GraphPad QuickCalcs (online). The sensitivity and specificity were determined for both the individual RCM parameters and the diagnosis. The gold standard was routine histology. Since only a very small number of lesions could be evaluated for Bowen's disease, a statistical analysis was considered unreasonable in this case. The zero hypothesis (H0) formulated for this study is that RCM and conventional histology result in different diagnoses. Accordingly, the alternative hypothesis (H1) assumes that RCM and histology yield consistent diagnoses. At a *P*-value of ≤.05 (error probability 5%), the result was considered statistically significant and the zero hypothesis (H0) was discarded. At a *P*-value of ≤.01, the result was rated very significant, and at a *P*-value of ≤.001 highly significant.^{43,44} Finally, it was checked whether the two investigators had made concordant diagnoses and found the same RCM parameters, respectively. The degree of concordance was expressed by Cohen's Kappa coefficient (*k*). The reliability was considered as follows: At a Kappa coefficient of 1.00-0.81, the interobserver concordance was very good; at 0.80-0.61, good; at 0.60-0.41, medium; at 0.40-0.21, slight; and at <0.20, weak according to Altman.⁴⁵

3 | RESULTS

3.1 | Morphological RCM analyses of basal cell carcinoma

Loss of honeycomb structure with slightly atypical keratinocytes: At the stratum granulosum (SG)/stratum spinosum level, a disordered keratinocyte pattern is visible (Figure 1A). It was caused by a chronic actinic skin damage. Dendritic cells: They are located within the tumor cell nests and the overlaying epidermis, respectively (Figure 1B). They are bright and have a star-shaped body. Their long, slender projections are strongly branched. Streaming: At the DEJ level, there is a uniform population of tumor cells with

elongated nuclei (Figure 1C). They are arranged along an axis. The overlying epidermis is pleomorph. Tumor cell islands with peripheral palisade arrangement of the external row of cell nuclei: In the dermis hyporeflexive, dark tumor silhouettes are visible that are surrounded by bright collagen clusters (Figure 1D). Gap formation between tumor cells and tumor stroma: A dark region separates the neoplastic cell aggregates from the fibrous stroma (Figure 1D). It contains amyloid and mazine plaques.^{25,29} Inflammatory infiltrate: It consists of small, bright, clearly distinguishable cells without nucleus which frequently appears in clusters (Figure 1E). Multiplication, strong winding, and dilatation of the blood vessels: Vessels become entangled between the tumor nests due to neoplastic angiogenesis (Figure 1F).³¹

3.2 | Statistical analyses of basal cell carcinoma

The first cohort exhibited 20 lesions with a clinical BCC diagnosis. Both investigators diagnosed all histologically ensured BCCs (10/10) correctly by RCM. INV I also recognized all non-BCC lesions (10/10) as such, whereas INV II evaluated two lesions (2/10) erroneously as BCC, although one of these lesions was an SCC and the other one a dermal nevus cell nevus (NZN). Thus, RCM confirmed the histological findings very well, at a sensitivity and specificity of 100% in the case of INV I. The chi-square analysis yielded a highly significant result (*P* < .0001). INV II reached a very good sensitivity of 100% and a good specificity of 80%. The result of the chi-square test proved to be highly significant (*P* = .0003). Using the Kappa analysis, Cohen's coefficient of *k* = 0.800 could be calculated and a good interobserver concordance be shown according to Altman. For the RCM parameter tumor cell islands, the analyses of INV I yielded a sensitivity and specificity of 100% (Table 1A). Consequently, if this criterion is found, the lesion can be diagnosed as BCC at highest probability. Highest sensitivity was also demonstrated for the loss of honeycomb structure, with the specificity being high as well (90%). However, the inflammatory infiltrate with only moderate values was of minor importance for both the specificity (60%) and the sensitivity (70%). The analyses of INV II also showed highly sensitive (100%) and very specific (80%) values for the loss of honeycomb structure (Table 1B). The multiplication, strong winding, and dilatation of the blood vessels showed highest sensitivity (100%) at a poor specificity of only 50%. Streaming yielded high sensitivity and specificity values of 90% and 80%, respectively. Except for the inflammatory infiltrate (*P* = .1775), INV I reached the significance level for all RCM criteria (Table 1C). The highest significance values were reached for the loss of honeycomb structure (*P* < .0001), the tumor cell islands (*P* < .0001), and the streaming (*P* = .0010). Also, INV II reached the highest *P*-value of .0003 for the loss of honeycomb structure. Except for the inflammatory infiltrate (*P* = .3613) and the dendritic cells (*P* = 1), INV II was able to reach the significance level for the remaining criteria. Except for the inflammatory infiltrate, good to medium concordance data could be reached for all RCM criteria (Table 1D). A good concordance according to Altman was achieved for the loss of honeycomb structure and for streaming.

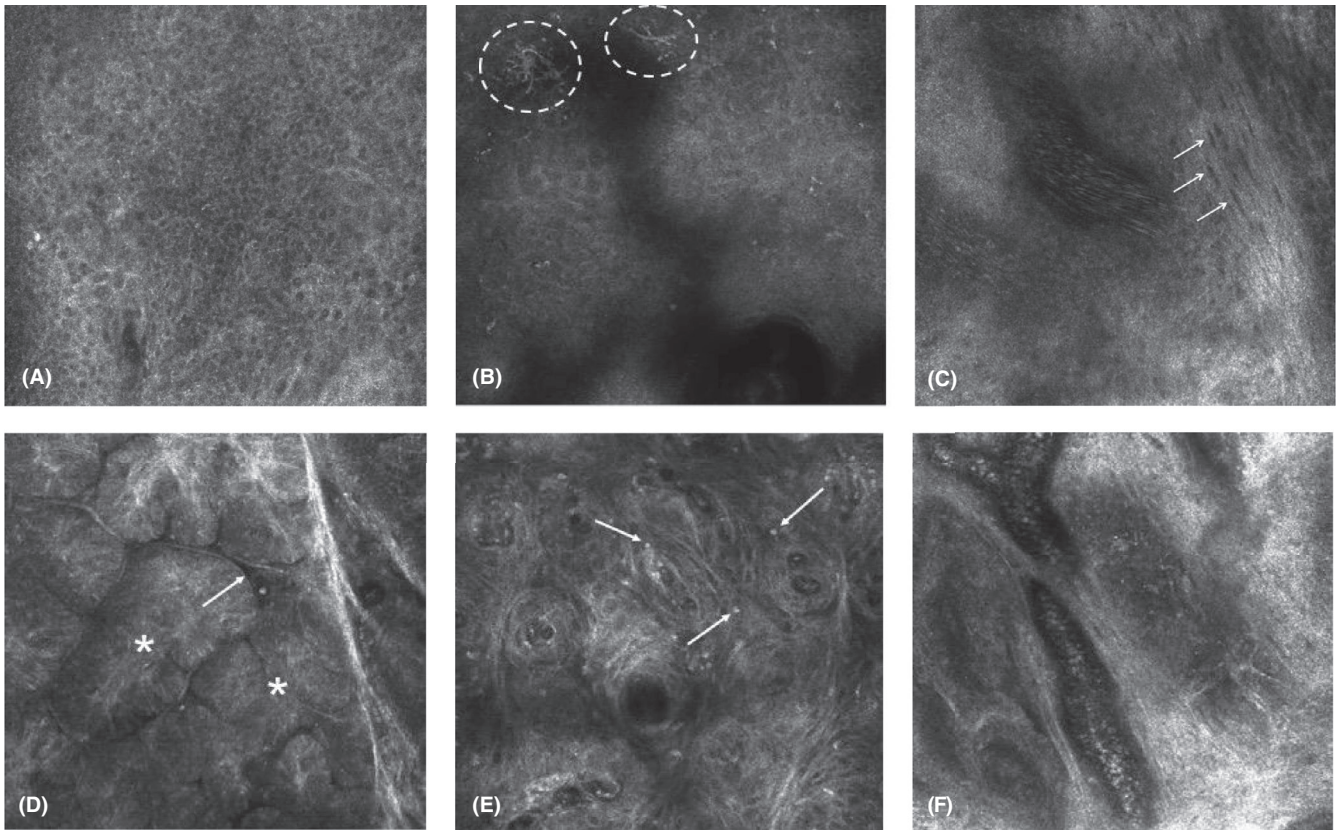


FIGURE 1 A, RCM image of SG/SS. A loss of the normal honeycomb structure is visible. B, RCM image of SG/SS showing two star-shaped dendritic cells (white dashed circles). C, RCM image at DEJ level showing dark, elongated cell nuclei polarizing along an axis (white arrows). D, RCM image of the dermis showing hyperreflective oval tumor cell nests (white stars), which are sharply delineated from the surrounding stroma by a dark, peritumoral gap (white arrow). E, The RCM image of the der DEJ/dermis shows an extensive inflammatory infiltrate in the form of numerous round, bright cells without nuclei (white arrows). F, RCM image at the level of the dermis. The increased diameter of one blood vessel is clearly visible

3.3 | Morphological RCM analyses of Bowen's disease

The RCM criteria of Bowen's disease are similar to those of AK. Therefore, only the parameters deviating from AK are described hereinafter. Strong loss of honeycomb structure with atypical keratinocytes: The loss of honeycomb structure is more pronounced, the cellular atypia can affect the entire epidermis (Figure 2A). Dyskeratotic cells: Within the atypical honeycomb pattern, two types of cells are observed. The first type is a large cell with bright center and dark halo; the second one, a large cell with dark center and bright border that is surrounded by a dark halo again (Figure 2B). In the histological findings, these cells correspond to the dyskeratotic keratinocytes with pyknotic nucleus. Increased vascularization/vascular dilatation: In the superficial papillary dermis, the vessels are visible as round-oval dilated regions; in the lower papillary dermis, they are s-shaped (Figure 2C).

The second cohort included six lesions with clinical diagnosis of Bowen's disease. Both investigators evaluated all of the lesions correctly. Unaware of histological diagnosis, both investigators correctly classified all lesions as Bowen's disease (4/4) detecting in two lesions that no MB was present (2/2). However, since only a very

small number of skin lesions could be evaluated in this clinical setting, no statistical analysis was conducted.

3.4 | Morphological RCM analyses of actinic keratosis

Single corneocytes detached from the cell cluster: The cell cluster of the SC is disturbed due to detaching corneocytes. The individual cells are bright and polygonal (Figure 3A). Parakeratosis: Due to a keratinization disorder, there are nuclei left in the corneocytes. The cells show a dark center and can be well distinguished from the stronger reflective cells of the SC (Figure 3B). Loss of honeycomb structure with atypical keratinocytes: In the SG/SS, the size and shape of the keratinocytes and their nuclei vary strongly; their cell borders appear irregular (Figure 3C). Dendritic cells: They appear isolated or in clusters and are frequently accompanied by an inflammatory infiltrate (Figure 3D). Inflammatory infiltrate: In inflammatory tissue, inflammatory cells migrating from the vascular system can be seen (Figure 3E). Increased vascularization/vascular dilatation: Moderately refractile erythrocytes flow in the central blood circulation at high speed, whereas the leukocytes slowly roll along

TABLE 1 Sensitivity and specificity analysis of (A) investigator I and (B) investigator II for the specific RCM parameters of basal cell carcinoma; (C) Results of the chi-square tests of both investigators for the specific RCM parameters of basal cell carcinoma; (D) Concordance rate for each RCM parameter of the basal cell carcinoma cohort

RCM parameter	Sensitivity (%)	Specificity (%)
(A) Sensitivity and specificity analysis of investigator I for the specific RCM parameters of basal cell carcinoma		
Loss of honeycomb structure with atypic keratinocytes	100	90
Dendritic cells	90	60
Streaming	100	70
Basaloid tumor nests with peripheral palisades	100	100
Peritumoral lacunae between the tumor islands and interstitial stroma	80	90
Inflammatory infiltrate	70	60
Enhanced vascularization or vascular dilatation	90	80
(B) Sensitivity and specificity analysis of investigator II for the specific RCM parameters of basal cell carcinoma		
Loss of honeycomb structure with atypic keratinocytes	100	80
Dendritic cells	50	50
Streaming	90	80
Basaloid tumor nests with peripheral palisades	90	60
Peritumoral lacunae between the tumor islands and interstitial stroma	90	60
Inflammatory infiltrate	50	70
Enhanced vascularization or vascular dilatation	100	50
RCM parameter	Investigator I	Investigator II
(C) Results of the chi-square tests of both investigators for the specific RCM parameters of basal cell carcinoma		
Loss of honeycomb structure with atypic keratinocytes	$P < .0001$	$P = .0003$
Dendritic cells	$P = .0191$	$P = 1$
Streaming	$P = .0010$	$P = .0017$
Basaloid tumor nests with peripheral palisades	$P < .0001$	$P = .0191$
Peritumoral lacunae between the tumor islands and interstitial stroma	$P = .0017$	$P = .0191$
Inflammatory infiltrate	$P = .1775$	$P = .3613$
Enhanced vascularization or vascular dilatation	$P = .0017$	$P = .0098$
RCM parameter	Cohen's kappa coefficient	Strength of concordance
(D) Concordance rate for each RCM parameter of the basal cell carcinoma cohort		
Loss of honeycomb structure with atypic keratinocytes	$k = 0.739$	Good according to Altman
Dendritic cells	$k = 0.528$	Moderate according to Altman
Streaming	$k = 0.700$	Good according to Altman
Basaloid tumor nests with peripheral palisades	$k = 0.466$	Moderate according to Altman
Peritumoral lacunae between the tumor islands and interstitial stroma	$k = 0.494$	Moderate according to Altman
Inflammatory infiltrate	$k = 0.346$	Mild according to Altman
Enhanced vascularization or vascular dilatation	$k = 0.564$	Moderate according to Altman

the vascular walls (Figure 3F). Solar elastosis: A moderate solar elastosis exhibits an unorganized, hyporefractile collagen in the reticular dermis (Figure 3G); if the damage is more severe, highly refractile curled fibers are visible (Figure 3H).

3.5 | Statistical analyses of actinic keratosis

The third cohort included 23 lesions with clinical AK diagnosis. Both INV correctly diagnosed 17 out of 18 histologically ensured AKs by using RCM. INV I evaluated the absence of AK in four out of five non-AK lesions correctly. However, an excoriation was erroneously evaluated by him as AK. INV II diagnosed the absence of AK in three out of five non-AK lesions; the lesions evaluated as AK by mistake were one Lichen planus and one verruca. Thus, a very good interobserver sensitivity of 94.4% for RCM could be demonstrated. INV I also reached a good specificity of 80%, while the specificity of INV II was only moderate (60%). According to the contingency test, the diagnosis of INV I proved to be highly significant ($P = .0004$), while a very significant result ($P = .0045$) was determined for INV II. Using the Kappa analysis, Cohen's coefficient of $k = 0.587$ was calculated which corresponds to a moderate concordance according to Altman. The analyses of INV I showed the highest sensitivity of 100% for the single corneocytes that were detached from the cell cluster, followed by the loss of honeycomb structure with 94.4% (Table 2A). For these criteria, a moderate (60%) and even a good specificity (80%), respectively, could be calculated. Parakeratosis and increased vascularization, however, were of minor importance for the diagnosis of AK. With 40% and 20%, respectively, the specificity obtained by INV I for these two criteria was only poor, although the sensitivity was high (77.8%). INV II could also show high sensitivity values for the loss of honeycomb structure (94.4%) and the single corneocytes detached from the cell cluster (83.3%) (Table 2B). However, the specificity calculated for these parameters was only moderate (60%). The inflammatory infiltrate and parakeratosis values found by INV II turned out to be highly specifically, amounting to 80%, each. For these parameters, also high sensitivity values of 88.9% and 77.8%, respectively, could be shown. The poorest specificity value of 20% was calculated for the increased vascularization, although the sensitivity was high (83.3%). INV I obtained with p -values of 0.0004 highly significant results for the loss of honeycomb structure and the individual corneocytes detached from the cell cluster, respectively (Table 2C). The dendritic cells and the solar elastosis turned out to be very significant, whereas the other criteria remained below the significance level. INV II showed for the inflammatory infiltrate and the loss of honeycomb structure P -values of .0019 and .0045, which are considered to be very significant. Although significant values were obtained for the individual detached corneocytes and parakeratosis, the zero hypothesis could not be discarded for the remaining parameters. A good interobserver concordance was shown for the dendritic cells (Table 2D), whereas the concordance regarding the loss of honeycomb structure was only low.

3.6 | Morphological RCM analyses of verruca

Single corneocytes detached from the cell cluster: The histological correlate to this corresponds to hyperkeratosis (Figure 4A). Koilocytosis: In the honeycomb pattern, large, balloon-shaped keratinocytes are pronounced. They are called koilocytes and occur in HPV infections. In histological findings, they correspond to vacuolated cells with basophilic nuclear inclusions (Figure 4B). Dendritic cells: They can occur in inflammatory verrucae at high density and represent an immune response of the body to a HPV infection (Figure 4C). Papillomatosis: At the DEJ level, monomorphic, bright, round cells are visible that are arranged around the darker dermal papillae. The diameter of the papillary bodies is wider, and their number and density are increased. The histological correlate thereof is the rete ridge lengthening and papillomatosis (Figure 4D).^{46,47} Increased vascularization/vascular dilatation: An increased amount of blood components can leak through the vessels into the SC. Therefore, the verrucae often appear darkish (Figure 4E).

3.7 | Statistical analyses of verruca

The last cohort included 12 lesions with clinically diagnosed verrucae. INV I failed to correctly diagnose one verruca out of seven (6/7) INV II, however, succeeded in diagnosing all histologically ensured verrucae (7/7) correctly. The absence of verruca was recognized by INV I for all non-verrucae lesions (5/5), and INV II misinterpreted only one lesion (4/5) as verruca, which was a fibroma, however. Thus, the findings of INV I showed a very good specificity of 100% and a good sensitivity of 85.7%. According to the contingency test, the diagnosis of INV I proved to be very significant ($P = .0034$), whereas INV II obtained a very good sensitivity of 100% and a good specificity of 80%. This result, too, proved to be very significant ($P = .0038$) in the contingency test. Using the Kappa analysis, Cohen's coefficient of $k = 0.667$ was calculated, corresponding to a good agreement according to Altman. With koilocytosis values of 100% and 85.7% and dendritic cell values of 100% and 71.4%, the findings of INV I turned out to be of highest specificity and very sensitive, respectively (Table 3A). Consequently, these RCM parameters are the most reliable ones for the diagnosis of verruca. Of minor importance is papillomatosis with moderate specificity (60%) and poor sensitivity (50%) results, respectively. INV II, however, was able to reach the highest sensitivity for koilocytosis at good specificity of 80% (Table 3B). Papillomatosis turned out to be neither especially sensitive (57.1%) nor particularly specific (20%). The contingency test yielded very significant koilocytosis results both for INV I ($P = .0034$) and for INV II ($P = .0038$) (Table 3C). For the single cells detached from the cell cluster, an interobserver significance level was reached with a P -value of .018, whereas for the dendritic cells a significance level was reached with P -value of .0133 by INV I and .0228 by INV II, respectively. Overall good to moderate concordances could be demonstrated for all criteria (Table 3D). Good agreement according to Altman was shown for the dendritic cell and increased vascularization parameters.

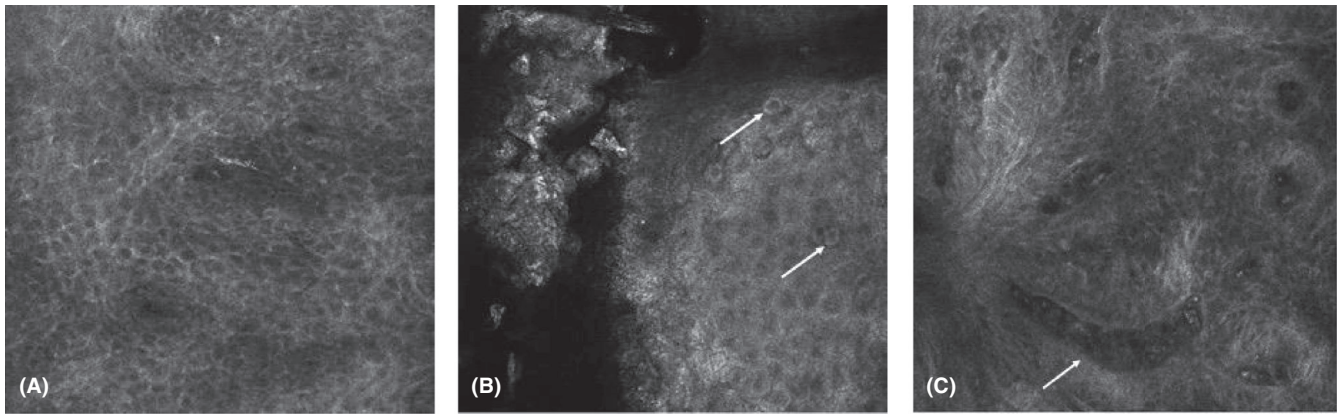


FIGURE 2 A, RCM image of SG/SS showing a strong loss of the normal honeycomb structure with pronounced architectural disorder. B, RCM image showing round cells with a dark center, a surrounding bright border and a dark halo (white arrows), which might probably correspond to dyskeratotic cells. C, RCM image of the dermis. Various dilated blood vessels are visible that are especially impressive at the bottom (white arrow)

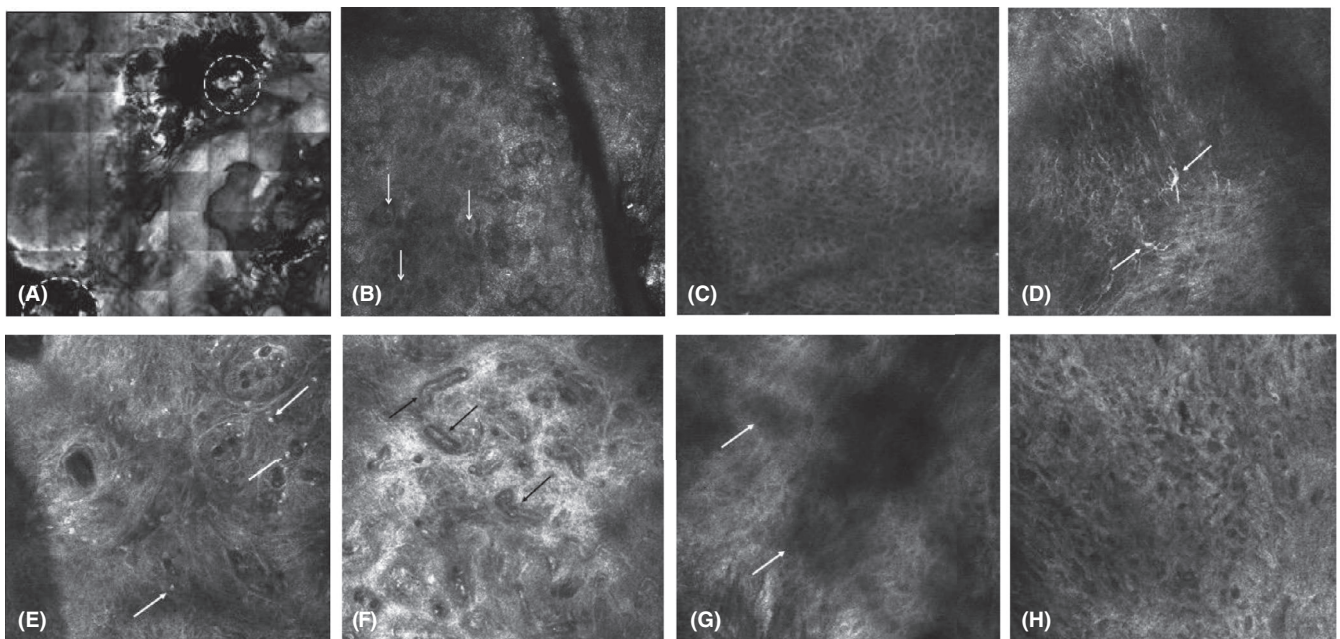


FIGURE 3 A, RCM overview image (4 x 4 mm) showing an interruption of the cell cluster. Single, detached corneocytes can be recognized (white dashed circles). B, RCM image showing multiple parakeratosis as polygonal, nucleus-containing cells with dark centers and sharp delineation to the SC (white arrows). C, RCM image of the SG/SS showing a loss of the normal honeycomb structure with pronounced architectural disorder by wide and blurred cell borders as well as atypia and pleomorphism of the keratinocytes. D, This image represents two prominent, star-shaped dendritic cell bodies (white arrows). E, RCM image of the dermal region exhibiting a pronounced perivascular inflammatory infiltrate. Numerous highly refractile round cells are visible (white arrows). F, Various longitudinal and cross sections through the vessels reveal their increased prevalence (black arrows). The blood cells within the vessel lumina are represented as being moderately refractile. G, RCM image at the level of the dermis showing an unorganized, hyporefractile collagen, whose single fibers are not visible (white arrows). H, RCM image at the level of the upper dermis showing highly refractile, curled fibers that are induced by severe UV damage

4 | DISCUSSION

According to our knowledge, data exclusively addressing the evaluation of neoplastic and virus-associated dermal diseases in organ transplanted patients have not been published, yet. However, there is a variety of partially clinical studies concerning the RCM criteria of these skin diseases in immunocompetent subjects.¹⁷⁻²⁴ As already

stated, many skin lesions in organ transplant recipients neither clearly meet the typical clinical criteria of the respective diseases nor do they exhibit the characteristic dermatoscopic criteria. Here, noninvasive RCM could be a useful tool to evaluate multiple lesions early without any time-consuming and expensive skin biopsies being necessary. A correct diagnosis of these diseases is indispensable for selecting the optimum treatment. While invasive surgery is the gold standard for most subtypes of BCC and Bowen's disease, noninvasive local

therapies are generally preferred for superficial BCCs, AKs, and verrucae. Consequently, noninvasive diagnostic tools should be developed, too.

4.1 | Basal cell carcinoma

In the literature, sensitivity values ranging between 48.8% and 100% and specificity values ranging between 53.6% and 100%, respectively, have been reported for BCC diagnosis by means of RCM.^{18,27,48} Nori et al determined in a large multicenter study for the presence of four RCM parameters a specificity of 95.7% and a sensitivity of 82.9%.¹⁸ This correlates well with the result of the present study. For the identification of four or more parameters, an interobserver sensitivity of 100% and a specificity of 100% (INV I) and 80% (INV II), respectively, were determined. Venturini et al investigated the sensitivity and specificity of RCM for the diagnosis of early subclinical BCC recurrences post-MAL-PDT, reaching 100%, each. According to the authors, the detection of tumor cell nests was sufficient for the diagnosis,⁴⁹ whereas Guitera et al evaluated 710 lesions and defined an algorithm from eight RCM parameters. If all criteria of the algorithm were met, a sensitivity of 100% and a specificity of 88.5% could be determined for the diagnosis.⁴⁸ In our study, the loss of honeycomb structure turned out to be the best parameter for BCC diagnosis. It showed an interobserver sensitivity of 100% and a specificity of 90% and 80%, respectively, as well as highest significance in the chi-square test. In addition, the Kappa analysis showed a good correlation, which supported the importance of this parameter further. On contrary, Nori et al published for this parameter a poorer sensitivity of 63.4% and a specificity of 63.8%.¹⁸ For the tumor cell nests, a high sensitivity of 100% and 90%, respectively, was obtained in the present study. This is in agreement with Webber et al, who reported a sensitivity of 91.6% when evaluating superficial BCCs for this parameter. The frequency value determined by the two investigators amounted to 100% and 90%, respectively (data not shown), which is similar to the findings of Rishpon et al (100%), Webber et al (100%) and Peppelman et al (97.6%).^{29,30,50} However, it is important to consider that the tumor cell nests in sclerodermiform BCCs tend toward being small and thin and are therefore hard to differentiate from the dermis, whereas they can appear bright in pigmented BCCs and stand out from the surrounding collagen only insufficiently. Therefore, it would be expected that advanced experience is required for their detection. However, the two investigators showed a medium interobserver concordance in the present study. Like Nori et al,¹⁸ both investigators reached with 100% and 90%, respectively, high sensitivity values for the streaming criterion, while the specificity fell slightly below (70% and 80%, respectively). Contrary to Longo et al, our analyses could show a good interobserver concordance for this criterion.^{28,29} In concordance with Nori et al, the two investigators obtained high sensitivity values of 90% and 100%, respectively, for the multiplication, strong winding, and dilatation of the blood vessels. As this is partially observed also in benign lesions such as verrucae or in inflammatory dermatoses such as psoriasis, the specificity strongly declined to 80% and 50%, respectively.⁵¹ These values also correlated very well

with Nori et al,¹⁸ who published a specificity of 53.6%. Referring to the gap formation between tumor cells and tumor stroma, Peppelman et al²⁹ stated an 80.5% prevalence in the lesions evaluated by them. Likewise, in that study high prevalences of 80% and 90%, respectively, were found for the peritumoral gap. On the other hand, the analyses of Rishpon et al reported these changes exclusively for every second BCC lesion.³⁰ Also the prevalences described by Longo et al,²⁸ with 77.3% in nodular and 13.6% in infiltrating BCCs are enlightening. According to our results, the most important RCM criteria for BCC diagnosis are the loss of honeycomb structure, the tumor cell nests, and streaming. We could show that the occurrence of these parameters in a lesion makes the presence of a BCC extremely possible. Moreover, it was demonstrated that RCM renders invasive biopsies unnecessary for most skin changes with the clinical diagnosis of a suspected BCC.

4.2 | Bowen's disease

Our small cohort of clinical Bowen's patients reflects the low prevalence of this dermal disease in the total population. Thus, there is only a limited number of studies, in which Bowen's disease was investigated in immunocompetent subjects by RCM.^{19,31-34} Only recently, Karaarslan et al³² presented the RCM criteria of the pigmented Bowen's disease based on a case study. Debarbieux et al³³ described three diagnostically challenging cases of pigmented Bowen's carcinoma, which were misinterpreted as melanoma due to the high density of dendritic cells. An investigation performed by Ulrich et al,¹⁹ which included these 10 cases of Bowen's disease, addressed the frequency of the RCM criteria. In all lesions, the authors could detect a strong loss of honeycomb structure (10/10). In the present study, this pattern was unanimously described by both investigators for all histologically ensured Bowen's lesions (4/4, data not shown). Dyskeratotic cells could be shown by Ulrich et al¹⁹ in five out of 10 lesions. This was in agreement with INV, who detected these cells in every second lesion; whereas INV II observed this parameter in only one lesion. These findings raise doubts as to whether this parameter can be reproduced for the diagnosis of Bowen's disease. The dendritic cells were visible in two (INV I) and three (INV II) of four lesions, respectively. Debarbieux et al, however, detected this cell type even in all lesions (3/3). This could be due to the fact that also the evaluated lesions are a specific subgroup of Bowen's disease that is clinically characterized by its pigmentation.³³ Although only a few lesions were analyzed, the present study demonstrates the usefulness of RCM for the diagnosis of Bowen's disease in immunosuppressed subjects and provides important data for future studies involving larger cohorts.

4.3 | Actinic keratosis

Horn et al²⁰ examined 30 flat AKs, reporting a sensitivity of 90.84% and a specificity of 77.50%. Similar to these results, in the present study an interobserver concordance was reached for the sensitivity with 94.4%, whereas the specificity was 80% (INV I) and 60% (INV II),

TABLE 2 Sensitivity and specificity analysis of (A) investigator I and (B) investigator I for the specific RCM parameters of actinic keratosis; (C) Results of the chi-square tests of both investigators for the specific RCM parameters of actinic keratosis; (D) Concordance rate for each RCM parameter of the actinic keratosis cohort

RCM parameter	Sensitivity (%)	Specificity (%)
(A) Sensitivity and specificity analysis of investigator I for the specific RCM parameters of actinic keratosis		
Single-detached keratinocytes	100	60
Parakeratosis	77.8	40
Loss of honeycomb structure with atypic keratinocytes	94.4	80
Dendritic cells	77.8	100
Inflammatory infiltrate	77.8	60
Enhanced vascularization or vascular dilatation	77.8	20
Solar elastosis	83.3	80
(B) Sensitivity and specificity analysis of investigator II for the specific RCM parameters of actinic keratosis		
Single-detached keratinocytes	83.3	60
Parakeratosis	77.8	80
Loss of honeycomb structure with atypic keratinocytes	94.4	60
Dendritic cells	77.8	60
Inflammatory infiltrate	88.9	80
Enhanced vascularization or vascular dilatation	83.3	20
Solar elastosis	66.7	60
RCM parameter	Investigator I	Investigator II
(C) Results of the chi-square tests of both investigators for the specific RCM parameters of actinic keratosis		
Single-detached keratinocytes	$P = .0004$	$P = .05$
Parakeratosis	$P = .4232$	$P = .0164$
Loss of honeycomb structure with atypic keratinocytes	$P = .0004$	$P = .0045$
Dendritic cells	$P = .0016$	$P = .1044$
Inflammatory infiltrate	$P = .1044$	$P = .0019$
Enhanced vascularization or vascular dilatation	$P = .9151$	$P = .8619$
Solar elastosis	$P = .0065$	$P = .2798$
RCM parameter	Cohen's kappa coefficient	Strength of concordance
(D) Concordance rate for each RCM parameter of the actinic keratosis cohort		
Single-detached keratinocytes	$k = 0.378$	Mild according to Altman
Parakeratosis	$k = 0.422$	Moderate according to Altman
Loss of honeycomb structure with atypic keratinocytes	$k = 0.151$	Low according to Altman
Dendritic cells	$k = 0.769$	Good according to Altman
Inflammatory infiltrate	$k = 0.334$	Mild according to Altman
Enhanced vascularization or vascular dilatation	$k = 0.6$	Moderate according to Altman
Solar elastosis	$k = 0.437$	Moderate according to Altman

respectively. For the AK diagnosis, four of the seven described RCM parameters had to be detected. Similarly, Ulrich et al¹⁷ reported in their study, which included 46 AK lesions, that the presence of four or five parameters can be sufficient for the diagnosis. In this work, the loss of honeycomb structure turned out to be the best RCM parameter with a sensitivity of 94.4% obtained by both investigators as well

as 80% and 60% specificity values obtained by INV I and INV II, respectively. Ulrich et al evaluated this parameter separately for the SG and the SS. The sensitivity calculated for the SG was 74.4%, whereas the calculation for the specificity yielded 100%. For the SS, the sensitivity even increased to 91.2%, which correlates with our results, whereas the specificity obtained by Ulrich et al declined to 95.2%.¹⁷

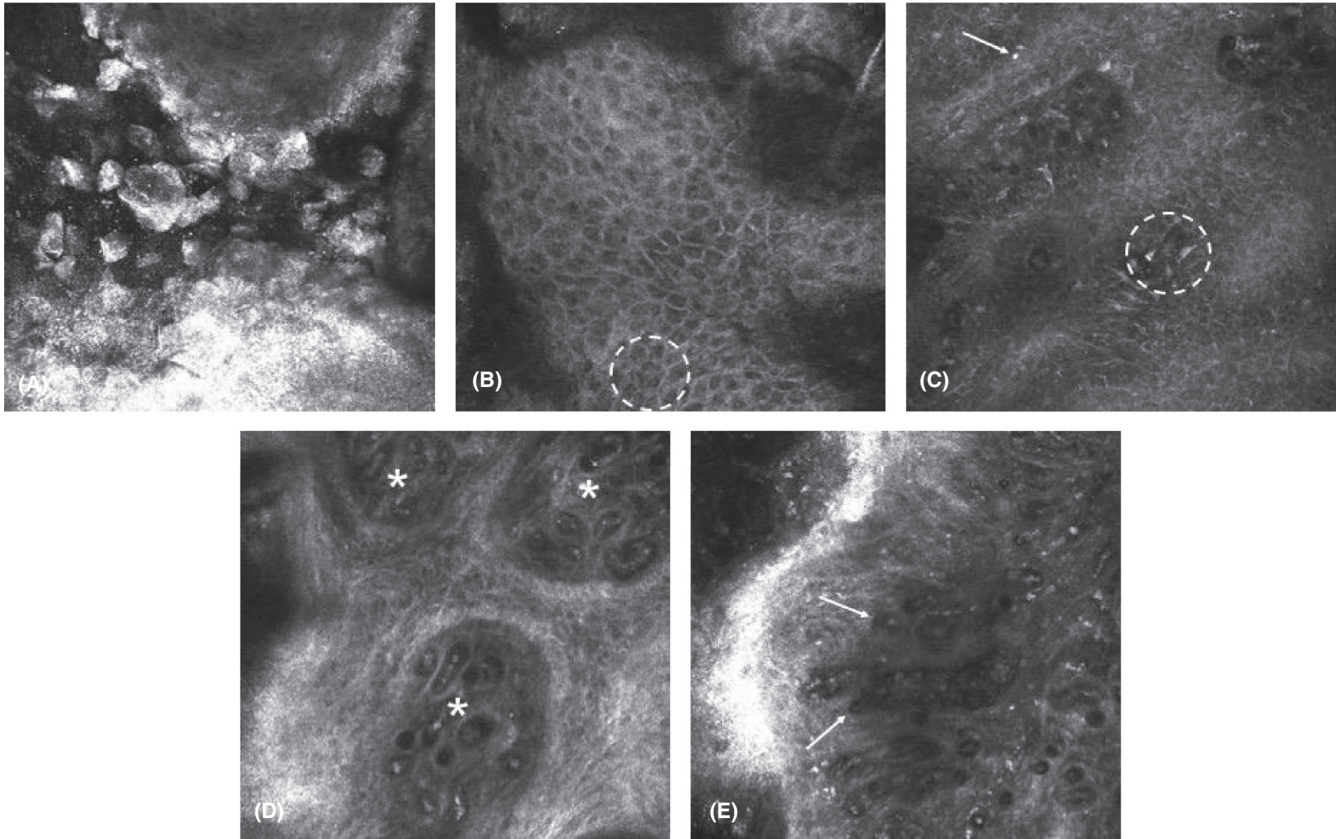


FIGURE 4 A, RCM image of the SC. Bright hornification cells detached from the homogenous cluster are visible. B, RCM image of the SS. At the bottom, a large, balloon-shaped keratinocyte can be seen (white dashed circle). C, The RCM image shows a massive infiltration of the SS by dendritic cells. Their cell bodies appear white (white dashed circle), and their extensions are strongly branched. They are accompanied by small, bright inflammatory cells (white arrow). D, RCM image at DEJ level. The dilated dermal papillae (white stars) appear dark. They are surrounded by monomorph, bright, round cells. In the papillae, numerous vascular sections are visible. E, RCM image at the level of the dermis. In the central region of the image, a prominent strongly dilated blood vessel can be seen, whose increased prevalence is illustrated by the white arrows

In our study, both investigators detected this criterion in 94.4% of the lesions (data not shown). Moscarella et al analyzed the morphology of 17 pigmented AKs and categorized the loss of honeycomb structure into two “sub-parameters.” Indeed, the authors observed atypical keratinocytes in 100% of the lesions, whereas an unorganized epidermal pattern was only described in 29.4%.⁵² Surprisingly, Horn et al subdivided this criterion even into five single parameters and always found lower prevalences compared with this study. Cohen’s coefficients for these parameters ranged from 0.4 to 0.6, apparently being more or less in concordance with our value of 0.151.²⁰ Here, it should be noted that for this criterion neither a clinical nor a dermatoscopic correlate can be assigned. Consequently, it is unique for the RCM evaluation. The single corneocytes detached from the cell cluster were identified as being the second-best parameter in the present study. The statistical analyses yielded high sensitivity values of 100% and 83.3%, respectively, whereas the 60% specificity obtained by both investigators was moderate. Ulrich et al observed for this parameter a similar sensitivity (98%) and a comparably higher specificity (71.4%).¹⁷ Probably, the presence of this RCM parameter as such is of limited diagnostic importance, as it can occur also in many benign lesions and inflammatory dermatoses, respectively. On the other hand,

it proved to be useful for diagnostics in constellation with other AK parameters, although its suitability is limited in the case of severe hyperkeratosis, as deeper epidermal and dermal structures, respectively, cannot be imaged. This is due to the high refractive index of the keratin in the superficial layers mostly consisting of scales and the resulting backscattering of light. Therefore, the RCM’s laser beam could occasionally not penetrate deeper than down to the SS, which forced us to remove the scales by curettage in some cases. In awareness of this problem, Ulrich et al proposed to use topic keratolytics for scale removal in future studies.⁵³ Referring to parakeratosis, a good interobserver sensitivity concordance of 77.8% was obtained, whereas only the result of INV II showed also a high specificity of 80% in the present study. The same sensitivity could be published by Ulrich et al, in addition to a higher specificity of 95.2% and a Kappa coefficient of 0.72. Contrary thereto, in our study only a *k*-value of 0.422 could be calculated for the nucleus-containing cells.¹⁷ In the present study, neither investigator reached significance level for the increased vascularization parameter in the contingency test. Thus, the detection of dilated vessels does not seem to be a sensitive marker for AK diagnostics. In agreement with Ulrich et al, our study suggests that the loss of honeycomb structure could present a key parameter for

TABLE 3 Sensitivity and specificity analysis of (A) investigator I and (B) investigator II for the specific RCM parameters of verruca; (C) Results of the chi-square tests of both investigators for the specific RCM parameters of verruca; (D) Concordance rate of both investigators for each RCM parameter of the verruca cohort

RCM parameter	Sensitivity (%)	Specificity (%)
(A) Sensitivity and specificity analysis of investigator I for the specific RCM parameters of verruca		
Single-detached keratinocytes	100	60
Koilocytosis	85.7	100
Dendritic cells	71.4	100
PM	50	60
Enhanced vascularization or vascular dilatation	42.9	80
(B) Sensitivity and specificity analysis of investigator II for the specific RCM parameters of verruca		
Single-detached keratinocytes	100	60
Koilocytosis	100	80
Dendritic cells	85.7	80
Papillomatosis	57.1	20
Enhanced vascularization or vascular dilatation	71.4	40
RCM parameter	Investigator I	Investigator II
(C) Results of the chi-square tests of both investigators for the specific RCM parameters of verruca		
Single-detached keratinocytes	$P = .018$	$P = .018$
Koilocytosis	$P = .0034$	$P = .0038$
Dendritic cells	$P = .0133$	$P = .0228$
Papillomatosis	$P = .7249$	$P = .4076$
Enhanced vascularization or vascular dilatation	$P = .4076$	$P = .6788$
RCM parameter	Cohen's kappa coefficient	Strength of concordance
(D) Concordance rate of both investigators for each RCM parameter of the verruca cohort		
Single-detached keratinocytes	$k = 0.437$	Moderate according to Altman
Koilocytosis	$k = 0.548$	Moderate according to Altman
Dendritic cells	$k = 0.625$	Good according to Altman
Papillomatosis	$k = 0.512$	Moderate according to Altman
Enhanced vascularization or vascular dilatation	$k = 0.640$	Good according to Altman

the diagnosis of AK.¹⁷ Future studies could help to identify particularly suitable combinations of RCM parameters that would render AK diagnostics even more reliable.

4.4 | Verruca

Erdoğan et al²² used RCM to monitor a verruca plantaris in vivo for its response to a therapy with a dye laser. Veasey et al²¹ studied the morphological RCM criteria of condylomata acuminata. Liu et al²⁴ addressed the differential diagnosis of verrucae planae and seborrheic keratoses, obtaining a sensitivity and specificity of 100%, each. In the present study, the diagnosis of verrucae yielded similar results, with highly significant sensitivity (85.7% and 100%) and specificity (100% and 80%), values, respectively, at simultaneously good interobserver concordance. The recently published study of Hui et al involved 55 patients with clinical verrucae planae. In all

evaluated verrucae, the authors observed bright papillary rings at the DEJ level (50/50).²³ However, as in the present study a dilated diameter and an increased number and density of dermal papillae were evaluated, a direct comparison seems problematic here. In 27 out of 55 lesions (49.1%), Hui et al²³ found petaloid structures in the SG/SS, which at most correlate with our koilocytosis parameter. In our study, the two investigators observed these structures almost twice as frequently (data not shown). In the contingency test, a statistical significance was established for this cell morphology. Thus, our results correlate with those of Liu et al,²⁴ who considered this parameter as main criterion for verrucae. Usually, verrucae are easy to diagnose with the bare eye. Due to aforementioned reasons, however, organ transplant recipients must occasionally be subjected to histology. For these patients, RCM as an optical method, which causes neither pain nor scars, could be a suitable tool for verifying clinical diagnoses or monitoring treatment processes.

4.5 | Limitations of the study

The evaluation of reflectance confocal microscopic images requires special education and experience. The level of experience and expertise can vary to a high extent depending on the investigator. Both investigators within this study were moderately to highly skilled at the evaluation of confocal images. Therefore, in clinical practice evaluation quality, sensitivity, and specificity might differ from the results found in our study.

Furthermore, during in vivo measurements the investigator will always be able to clinically evaluate the lesion, which may easily bias the microscopic evaluation.

The deeper the structure under investigation, the lower is the resolution of confocal images. For example, tumor nests located deeper than 350 μm , which can occur in nodular, and micronodular basal cell carcinoma could not be visualized by reflectance confocal microscopy. Another limitation of confocal imaging is hyperkeratosis due to the high index of refraction of keratin, with the resulting backscattering of light, which limits the optical penetration depth of RCM.

5 | CONCLUSION

The present study involving larger cohorts of patients has been the first to use RCM for analyzing neoplastic and virus-associated skin changes in organ transplant recipients. It proved to be a well reproducible and reliable method for the diagnosis of BCCs and AKs. The study has already resulted in a very good definition of RCM parameters permitting a specific diagnosis of these skin diseases. RCM could provide a huge potential as a genuine alternative to histological diagnostics by invasive skin biopsy. Due to the few numbers of patients with Bowen's disease investigated by us, a conclusion is difficult. It must be taken into account, however, that this disease is a rare one. Although verrucae occur relatively often and are easily detectable, it has to be considered that multiple new hyperkeratotic lesions often occur under immunosuppression, where verrucae, but also epithelial tumors, such as in situ or invasive SCC, have to be considered as differential diagnosis. In this context, RCM represents a valuable diagnostic tool that may provide important information complementing clinical or dermatoscopic findings. There is no doubt that RCM plays and will continue to play a central role in the diagnostics of neoplastic and virus-associated skin diseases in organ transplant recipients.

ORCID

Sora Jung  <https://orcid.org/0000-0002-9520-2750>

REFERENCES

- Hofbauer G. Immunosuppressive therapy after transplantation. Dermatologic relevance and pathomechanisms. *Hautarzt*. 2010;61(3):214-219.
- Leiter U, Garbe C. Skin cancer in organ transplant patients. Epidemiology and management. *Hautarzt*. 2010;61(3):207-213.
- Lonsdorf AS, Becker MR, Stockfleth E, Schäkel K, Ulrich C. Primary and secondary prevention of skin cancer in organ transplant recipients. *Hautarzt*. 2010;61(3):195-206.
- Ulrich C, Christophers E, Sterry W, Meyer T, Stockfleth E. Skin diseases in organ transplant patients. *Hautarzt*. 2002;53(8):524-533.
- Ulrich C, Stockfleth E. Empfehlungen für die Diagnostik und Therapie weiterer Tumoren: Hauttumoren bei Immunsuppression - Dermatologie bei Organtransplantierten. In: Szeimies R-M, Hauschild A, Garbe C, Kaufmann R, Landthaler M, eds. *Tumoren der Haut: Grundlagen, Diagnostik und Therapie in der Dermatologischen Onkologie*, 1st edn. Stuttgart, Germany: Georg Thieme; 2010:647-652.
- Fernandes AR, Santos AC, Sanchez-Lopez E, et al. Neoplastic multifocal skin lesions: biology, etiology, and targeted therapies for nonmelanoma skin cancers. *Skin Pharmacol Physiol*. 2018;31(2):59-73.
- Hogewoning AA, Goettsch W, van Loveren H, de Fijter JW, Vermeer BJ, Bouwes Bavinck JN. Skin infections in renal transplant recipients. *Clin Transplant*. 2001;15(1):32-38.
- Hiesse C, Rieu P, Kriaa F, et al. Malignancy after renal transplantation: analysis of incidence and risk factors in 1700 patients followed during a 25-year period. *Transplant Proc*. 1997;29(1-2):831-833.
- Kaufmann R, Linhart C, Wolter M. Empfehlungen für die Diagnostik und Therapie des Basalzellkarzinoms: Diagnostik. In: Szeimies R-M, Hauschild A, Garbe C, Kaufmann R, Landthaler M, eds. *Tumoren der Haut: Grundlagen, Diagnostik und Therapie in der dermatologischen Onkologie*, 1st edn. Stuttgart: Georg Thieme; 2010:483-491.
- Breuninger H, Eigentler T, Bootz F, et al. S2k-Leitlinie 032/022: Plattenepithelkarzinom der Haut. AWMF online: Das Portal der wissenschaftlichen Medizin. <https://www.awmf.org/leitlinien/detail/II/032-022.html>. Published 2013. Accessed June 21, 2018.
- Batz S, Wahrlich C, Alawi A, Ulrich M, Lademann J. Differentiation of different nonmelanoma skin cancer types using OCT. *Skin Pharmacol Physiol*. 2018;31(5):238-245.
- Krüger-Corcoran D, Stockfleth E, Jürgensen JS, et al. Human papillomavirus-associated warts in organ transplant recipients. Incidence, risk factors, management. *Hautarzt*. 2010;61(3):220-229.
- Hartevelt MM, Bavinck JN, Kootte AM, Vermeer BJ, Vandenbroucke JP. Incidence of skin cancer after renal transplantation in The Netherlands. *Transplantation*. 1990;49(3):506-509.
- Stockfleth E, Kerl H, Guideline Subcommittee of the European Dermatology Forum. Guidelines for the management of actinic keratoses. *Eur J Dermatol*. 2006;16(6):599-606.
- Kolm I, Braun RP. How reflectance confocal microscopy works. In: Hofmann-Wellenhof R, Pellacani G, Malvehy J, Soyer HP, eds. *Reflectance Confocal Microscopy for Skin Diseases*. Berlin Heidelberg: Springer; 2012:7-10.
- Gareau DS, Patel YG, Rajadhyaksha M. Basic principles of reflectance confocal microscopy. In: González S, Gill M, Halpern AC, eds. *Reflectance Confocal Microscopy of Cutaneous Tumors: An Atlas with Clinical, Dermoscopic and Histological Correlations*, 1st edn. London, UK: Informa Healthcare; 2008:1-6.
- Ulrich M, Maltusch A, Rius-Díaz F, et al. Clinical applicability of in vivo reflectance confocal microscopy for the diagnosis of actinic keratoses. *Dermatol Surg*. 2008;34(5):610-619.
- Nori S, Rius-Díaz F, Cuevas J, et al. Sensitivity and specificity of reflectance-mode confocal microscopy for in vivo diagnosis of basal cell carcinoma: a multicenter study. *J Am Acad Dermatol*. 2004;51(6):923-930.
- Ulrich M, Kanitakis J, González S, Lange-Asschenfeldt S, Stockfleth E, Roewert-Huber J. Evaluation of Bowen disease by in vivo reflectance confocal microscopy. *Br J Dermatol*. 2012;166(2):451-453.

20. Horn M, Gerger A, Ahlgrimm-Siess V, et al. Discrimination of actinic keratoses from normal skin with reflectance mode confocal microscopy. *Dermatol Surg.* 2008;34(5):620-625.
21. Veasey JV, de Framil VM, Nadal SR, Marta AC, Lellis RF. Genital warts: comparing clinical findings to dermatoscopic aspects, in vivo reflectance confocal features and histopathologic exam. *An Bras Dermatol.* 2014;89(1):137-140.
22. Erdoğan S, Dorittke P, Kardorff B. Pulsed dye laser (FPDL) treatment of a plantar verruca vulgaris and in vivo monitoring of therapy with confocal laser scan microscopy (CLSM). *J Dtsch Dermatol Ges.* 2013;11(8):760-762.
23. Hui D, Hong-Yan J, Ai-E X. Evaluation of verruca plana by in vivo reflectance confocal microscopy and dermoscopy. *Skin Res Technol.* 2017;23(3):437-440.
24. Liu H, Chen S, Zhang F, et al. Seborrheic keratosis or verruca plana? A pilot study with confocal laser scanning microscopy. *Skin Res Technol.* 2010;16(4):408-412.
25. González S, Tannous Z. Real-time, in vivo confocal reflectance microscopy of basal cell carcinoma. *J Am Acad Dermatol.* 2002;47(6):869-874.
26. Ahlgrimm-Siess V, Horn M, Koller S, Ludwig R, Gerger A, Hofmann-Wellenhof R. Monitoring efficacy of cryotherapy for superficial basal cell carcinomas with in vivo reflectance confocal microscopy: a preliminary study. *J Dermatol Sci.* 2009;53(1):60-64.
27. Curchin CES, Wurm EMT, Lambie DL, Longo C, Pellacani G, Soyer HP. First experiences using reflectance confocal microscopy on equivocal skin lesions in Queensland. *Australas J Dermatol.* 2011;52(2):89-97.
28. Longo C, Lallas A, Kyrgidis A, et al. Classifying distinct basal cell carcinoma subtype by means of dermatoscopy and reflectance confocal microscopy. *J Am Acad Dermatol.* 2014;71(4):716-724. e1.
29. Peppelman M, Wolberink EAW, Blokk WAM, van de Kerkhof PCM, van Erp PEJ, Gerritsen M-JP. In vivo diagnosis of basal cell carcinoma subtype by reflectance confocal microscopy. *Dermatol Basel Switz.* 2013;227(3):255-262.
30. Hashemi P, Rabinovitz HS, Marghoob AA, Scope A. Basal cell carcinoma. In: Hofmann-Wellenhof R, Pellacani G, Malvehy J, Soyer HP, eds. *Reflectance Confocal Microscopy for Skin Diseases.* Berlin Heidelberg, Germany: Springer; 2012:271-284.
31. Ulrich M, Lange-Asschenfeldt S, González S. In vivo reflectance confocal microscopy for early diagnosis of nonmelanoma skin cancer. *Actas Dermosifiliogr.* 2012;103(9):784-789.
32. Karaarslan I, Tepret S, Yildiz S, Yaman B, Ozdemir F. The role of reflectance confocal microscopy in a case of Bowen's disease difficult to diagnose. *Dermatol Pract Concept.* 2018;8(1):63-65.
33. Debarbieux S, Perrot JL, Cinotti E, et al. Reflectance confocal microscopy of Pigmented Bowen's disease: misleading dendritic cells. *Skin Res Technol.* 2017;23(1):126-128.
34. Braga JCT, Paschoal FM, Blumetti TCM, et al. Hypomelanotic melanoma mimicking pigmented Bowen disease. *J Am Acad Dermatol.* 2016;74(1):e11-e13.
35. Ulrich M, Maltusch A, Röwert-Huber J, et al. Actinic keratoses: non-invasive diagnosis for field cancerisation. *Br J Dermatol.* 2007;156(Suppl 3):13-17.
36. Ulrich M, Krueger-Corcoran D, Roewert-Huber J, Sterry W, Stockfleth E, Astner S. Reflectance confocal microscopy for non-invasive monitoring of therapy and detection of subclinical actinic keratoses. *Dermatology.* 2010;220(1):15-24.
37. Longo C, Casari A, De Pace B, Simonazzi S, Mazzaglia G, Pellacani G. Proposal for an in vivo histopathologic scoring system for skin aging by means of confocal microscopy. *Skin Res Technol.* 2013;19(1):e167-e173.
38. Welzel J, Ulrich M, Lange-Asschenfeldt S, Stolz W, Sattler E. S1-Leitlinie 013-076: Konfokale Lasermikroskopie in der Dermatologie. AWMF online: Das Portal der wissenschaftlichen Medizin. <https://www.awmf.org/leitlinien/detail/ll/013-076.html>. Published 2017. Accessed August 21, 2018.
39. Astner S, Ulrich M. Confocal laser scanning microscopy. *Hautarzt.* 2010;61(5):421-428.
40. Calzavara-Pinton P, Longo C, Venturini M, Sala R, Pellacani G. Reflectance confocal microscopy for in vivo skin imaging. *Photochem Photobiol.* 2008;84(6):1421-1430.
41. Lademann J, Knorr F, Patzelt A, et al. Laser scanning microscopic investigations of the decontamination of soot nanoparticles from the skin. *Skin Pharmacol Physiol.* 2018;31(2):87-94.
42. Technik: Hardware. MAVIG VivaScope. <http://www.vivascope.de/konfokale-laserscanmikroskopie/technik/hardware.html>. Accessed June 21, 2018.
43. Fletcher RH, Fletcher SW. *Klinische Epidemiologie: Grundlagen Und Anwendung*, 2nd edn. Bern, Switzerland: Hans Huber; 2007.
44. Hilgers R-D, Bauer P, Scheiber V. *Einführung in Die Medizinische Statistik*, 2nd edn. Berlin Heidelberg, Germany: Springer; 2007.
45. Altman DG. *Practical Statistics for Medical Research*. Boca Raton, London, New York, Washington, DC: Chapman and Hall/CRC Texts in Statistical Science; 1990.
46. Stadler R, Hartig C. Epidermale tumoren. In: Kerl H, Garbe C, Cerroni L, Wolff HH, eds. *Histopathologie Der Haut*, 1st edn. Berlin Heidelberg, Germany: Springer; 2003:543-585.
47. Ossadnik K, Philipp S, Bost W, Fournelle M, Richter H, Lademann J. Application of photoacoustic methods and confocal microscopy for monitoring of therapeutic response in plaque psoriasis. *Skin Pharmacol Physiol.* 2018;31(6):308-315.
48. Guitera P, Menzies SW, Longo C, Cesinaro AM, Scolyer RA, Pellacani G. In vivo confocal microscopy for diagnosis of melanoma and basal cell carcinoma using a two-step method: analysis of 710 consecutive clinically equivocal cases. *J Invest Dermatol.* 2012;132(10):2386-2394.
49. Venturini M, Sala R, González S, Calzavara-Pinton PG. Reflectance confocal microscopy allows in vivo real-time noninvasive assessment of the outcome of methyl aminolaevulinate photodynamic therapy of basal cell carcinoma. *Br J Dermatol.* 2013;168(1):99-105.
50. Webber SA, Wurm EMT, Douglas NC, et al. Effectiveness and limitations of reflectance confocal microscopy in detecting persistence of basal cell carcinomas: a preliminary study. *Australas J Dermatol.* 2011;52(3):179-185.
51. Archid R, Duerr HP, Patzelt A, et al. Relationship between histological and clinical course of psoriasis: a pilot investigation by reflectance confocal microscopy during Goeckerman treatment. *Skin Pharmacol Physiol.* 2016;29(1):47-54.
52. Moscarella E, Rabinovitz H, Zalaudek I, et al. Dermoscopy and reflectance confocal microscopy of pigmented actinic keratoses: a morphological study. *J Eur Acad Dermatol Venereol.* 2015;29(2):307-314.
53. Ulrich M, Astner S. Actinic keratosis. In: Hofmann-Wellenhof R, Pellacani G, Malvehy J, Soyer HP, eds. *Reflectance Confocal Microscopy for Skin Diseases.* Berlin Heidelberg, Germany: Springer; 2012:285-295.

How to cite this article: Rueter L, Ramadori P, Ulrich M, Jung S, Kardorff B, Lademann J. Reflectance confocal microscopy for noninvasive examination of nonmelanocytic tumors and virus-associated skin lesions in organ transplant recipients. *Skin Res Technol.* 2020;26:376-389. <https://doi.org/10.1111/srt.12813>